NANOSYSTEMS: PHYSICS, CHEMISTRY, MATHEMATICS, 2013, 4 (5), P. 696–705

# INFLUENCE OF SYNTHESIS TEMPERATURE ON $BiFeO_3$ NANOPARTICLES FORMATION

N. A. Lomanova[1], V. V. Gusarov[1,2]

[1]Ioffe Physical Technical Institute, 26 Polytekhnicheskaya Str.,
St. Petersburg 194021, Russian Federation
[2]St. Petersburg State Technological Institute (Technical University),
26 Moskovsky Ave., St. Petersburg, 190013, Russian Federation
natus@hotbox.ru, victor.v.gusarov@gmail.com

**PACS 61.66.Fn**

The mechanism of $BiFeO_3$ nanoparticle formation from initial compositions obtained by bismuth and iron hydroxides co-precipitation has been studied. The activation temperature of the $BiFeO_3$ nucleation and nanocrystal growth is shown to correlate with that of the nonautonomous phase's melting. The optimal temperature range during nanoparticle formation by the method in question was found to be between 460–520($\pm$40) °C.

**Keywords:** nanoparticles, multiferroics, bismuth ferrite, high-temperature X-ray diffractometry.

## 1. Introduction

Primarily, $BiFeO_3$–based materials are of interest as multiferroics used for the development of magnetoelectric materials and photovoltaics, including thin-film materials, nanostructures and compounds with $BiFeO_3$ nanosized blocks [1–10]. $BiFeO_3$ nanoparticles may have other potential applications, for example in [11] $BiFeO_3$ nanoparticles were used for $BiFeO_3$–graphene nanohybrids, which may find application due to their photocatalytic properties.

A wide range of investigations reviewed were devoted to the synthesis of $BiFeO_3$ by applying different methods and determining the optimal conditions for producing this compound free from other impurity phases [12]. Nevertheless, obtaining a pure single-phase product has been problematic, so far. Various authors have suggested different reasons for this. Some works describing the synthesis of $BiFeO_3$ synthesis mention its metastability as a reason for the inability to produce this compound uncontaminated by other components of the $Bi_2O_3$–$Fe_2O_3$ system (see, e.g., [13]). However, this is an equilibrium compound according to works on phase equilibria [14–17].

The difficulty of producing $BiFeO_3$ free from other phases by means of a solid phase synthesis was explained by its nonstoichiometry and changes in the homogeneity region with increased temperature [18]. In the same work, the activation of $BiFeO_3$ formation was shown to depend on the chemical background of the initial mixture. In this case, a number of subsequent transformations occur when $BiFeO_3$ is synthesized from $Bi_2O_3$ and $Fe_2O_3$ by the solid state chemical reaction method. At the initial stage, the formation of $Bi_{25}FeO_{39}$ takes place. Its maximum quantity was recorded at 500 °C. Then, $BiFeO_3$ synthesis intensified sharply at about 600 °C, and the further increase in the reaction temperature leads to the formation of $Bi_2Fe_4O_9$ along with $BiFeO_3$ and $Bi_{25}FeO_{39}$.

The possibility of $Bi_2Fe_4O_9$ and $Bi_{25}FeO_{39}$ formation during $BiFeO_3$ synthesis was shown to be dependent upon the quality of the initial reagents [19]. Insufficiently pure precursors resulted in the formation of the above-mentioned phases and to their stable existence as impurities during $BiFeO_3$ formation. Some authors postulate that it is difficult to synthesize the

single-phase $BiFeO_3$ because $Bi_2Fe_4O_9$ and $Bi_{25}FeO_{39}$ are thermodynamically more stable than $BiFeO_3$ [20, 21].

According to data from [22], thermodynamic calculations have yielded a conclusion that synthesis for the production of single-phase $BiFeO_3$ should not be performed above 727 °C, that is, above the temperature of the $\alpha \rightarrow \beta$ $Bi_2O_3$ transition, as the high entropy of the disordered $\beta$-$Bi_2O_3$ sharply decreases the Gibbs energy of bismuth ferrite formation. The suggested optimal synthesis temperature is around 720 °C.

A schematic description of $BiFeO_3$, as well as $Bi_2Fe_4O_9$ and $Bi_{25}FeO_{39}$ impurities formation has been given previously [23]. The diffusion of $Bi^{3+}$ ions through $Fe_2O_3$ was shown to have a decisive role in $BiFeO_3$ synthesis. However, the diffusion of components into the reaction zone was hindered by the crystallization of the $Bi_2Fe_4O_9$ phase, which is more thermodynamically stable.

A detailed analysis of $BiFeO_3$ synthesis provided in [24] showed that when $BiFeO_3$ was synthesized from a xerogel, its crystallization started above 520 °C, which is more than 100 °C below the temperature of its synthesis from simple oxides by applying the solid state chemical reaction method with mechanochemical activation of components [25]. In this case, practically no formation of the intermediate phase $Bi_{25}FeO_{39}$ was observed, and the yield of $BiFeO_3$ at 580 °C was 99.7 mass %, which was maintained over a wide temperature range.

Synthestic methods for obtaining $BiFeO_3$ nanoparticles have been considered in many publications. Several works describe the production of $BiFeO_3$ nanoparticles of various sizes and morphologies applying low temperature techniques, including the hydrothermal technique [25–32].

The details regarding the formation, structure and size of $BiFeO_3$ nanoparticles synthesized from different precursors were studied in [33,34]. It was demonstrated in [34] that $BiFeO_3$ crystallization begins around 400 °C, and, according to these publications, an increase in the reaction temperature of up to 500–600 °C may yield single-phase $BiFeO_3$.

Various methods for synthesizing $BiFeO_3$ nanoparticleswere described, which, however, did not yield monophase nanopowders [35–39]. The published data analysis showed a lack of certainty in the interpretation of the reasons for the multiphase nature of the system during $BiFeO_3$ synthesis. This relates to the synthesis of both $BiFeO_3$ macroparticles and nanoparticles. Therefore, investigation of the mechanistic details of $BiFeO_3$ nanoparticle formation is topical.

## 2. Experimental

$BiFeO_3$ nanoparticles were synthesized by means of thermal treatment of hydroxides obtained by reverse co-precipitation from solutions of salts into a 25% solution of $NH_4OH$. The purities of the starting materials, $Bi(NO_3)_3 \cdot 5H_2O$ and $Fe(NO_3)_3 \cdot 9H_2O$, were 99.9% or higher. The concentration of bithmus and iron (III) nitrates was 0.1 M/l and dilute nitric acid was used as the solvent. Solutions of the salts were mixed in a ratio corresponding to $BiFeO_3$ stoichiometry. The coprecipitated mixture was washed with distilled water until the presence of ammonium ions was not detected. The precipitate was dried at about 70 °C for 2 hours.

The elemental composition of the studied samples was determined by the energy dispersive X-ray microanalysis (FEI Quanta 200 SEM with the EDAX attachment) prior to and after their thermal treatment. The changes induced in the samples by thermal treatment were studied by the simultaneous thermal analysis (STA) using STA 449 F3 Jupiter (NETZSCH), as well as by the high-temperature X-ray diffractometry (HT-XRD) employing XRD-7000 Shimadzu with HTK–1200N high-temperature attachment (Anton Paar).

The sample investigated by HT-XRD was heated in a stepwise manner from 480–630 °C and was subjected to isothermal exposure for 5–7 min before diffractogram recording. The

X-ray quantitative phase analysis (XQPA) employed the PDWin 4.0 code [40]. The material of the tray in which the sample was placed ($\alpha$-$Al_2O_3$) was used as the internal standard. The coherent scattering domain size was determined using the Scherrer equation. A correction for the X-ray line broadening (independent of the particle size) was made using the data on the $\alpha$-$Al_2O_3$ line width.

## 3. Results and discussion

According to the elemental analysis data for the initial sample composed of coprecipitated bismuth and iron hydroxides and dried at ~70 °C, the elemental ratio corresponded to $BiFeO_3$ stoichiometry; Fe:Bi = 1.08±0.05. Elemental analysis data obtained after the HT-XRD for the sample heated in a stepwise manner up to 630 °C was shown to decrease in bismuth oxide content, which may be due to its evaporation (Fe:Bi = 1.47±0.05).

The HT-XRD of the initial sample (Fig. 1a) demonstrated the presence of only broad $Bi(OH)_3$ reflections in the diffractogram, which correspond to 30–35 nm crystallites. The absence of reflections for any other phases in the diffractogram obviously relates to the presence of an amorphous iron-containing component. It should be noted that according to [41], the amorphous state is characteristic of iron hydroxide precipitated in an alkaline medium.

A comparison of the HT-XRD (Fig. 1) and STA (Fig. 2) data makes it possible to present phase changes in the sample as a below-described series of transformations. Within the 40–160 °C range, dehydration of ferric oxyhydroxide yields an amorphous iron oxide. This dehydration temperature range corresponds to that published in [41]. This process is reflected in the TG and DSC curves as a loss in sample mass (1.8 %), and as a small and temperature-expanded endothermic effect (11 J/g). Mass-spectrometry of the evolving gases proved the process to be dehydration (Fig. 2).

Within the 160–300 °C range, the sample keeps losing mass due to $Bi(OH)_3$ dehydration and to decomposition of a small amount of carbonate, which is accompanied by the loss of 4 % of mass (Fig. 2). This process occurs simultaneously with the chemical reaction of iron oxide with the sillenite-structure bismuth, which is usually presented as the compound $Bi_{25}FeO_{39}$ or $Bi_{25}FeO_{40}$ [42]. The total endothermic effect with an enthalpy of 147 J/g corresponds to the mentioned processes.

Obviously, decomposition of the bismuth carbonate impurity accompanied by the loss of 2 % of mass and by the endothermic effect with enthalpy of 41 J/g were observed between 320–500 °C. Completion of this process was immediately followed by $BiFeO_3$ formation with the corresponding exothermic effect with an enthalpy of –30 J/g.

Notable are the small differences between the data generated by HT-XRD and STA due to the idiosyncrasies of these techniques. Firstly, in HT-XRD, all processes are registered at lower temperatures than in STA. The reason is that the latter technique is dynamic, and therefore, it is more difficult to register the onset of a transformation with its help due to the final rate of temperature growth. On the other hand, the STA data make it possible to register the transformation of amorphous phases, while this is impossible with the HT-XRD data. Besides, HT-XRD requires a sufficiently long exposure of samples at each stage of the high-temperature measurements, which increases the possibility of shifts in the quantitative ratio of initial components due to the evaporation of the volatile bismuth oxide.

The results of XQPA (performed with due account of the mass balance , numerical data on the X-ray density of the crystal-forming phases and the data on the size of the crystallites in them) made it possible to determine volume fractions of the formed crystal phases, the volume of crystallites and their relative quantity (Fig. 3).

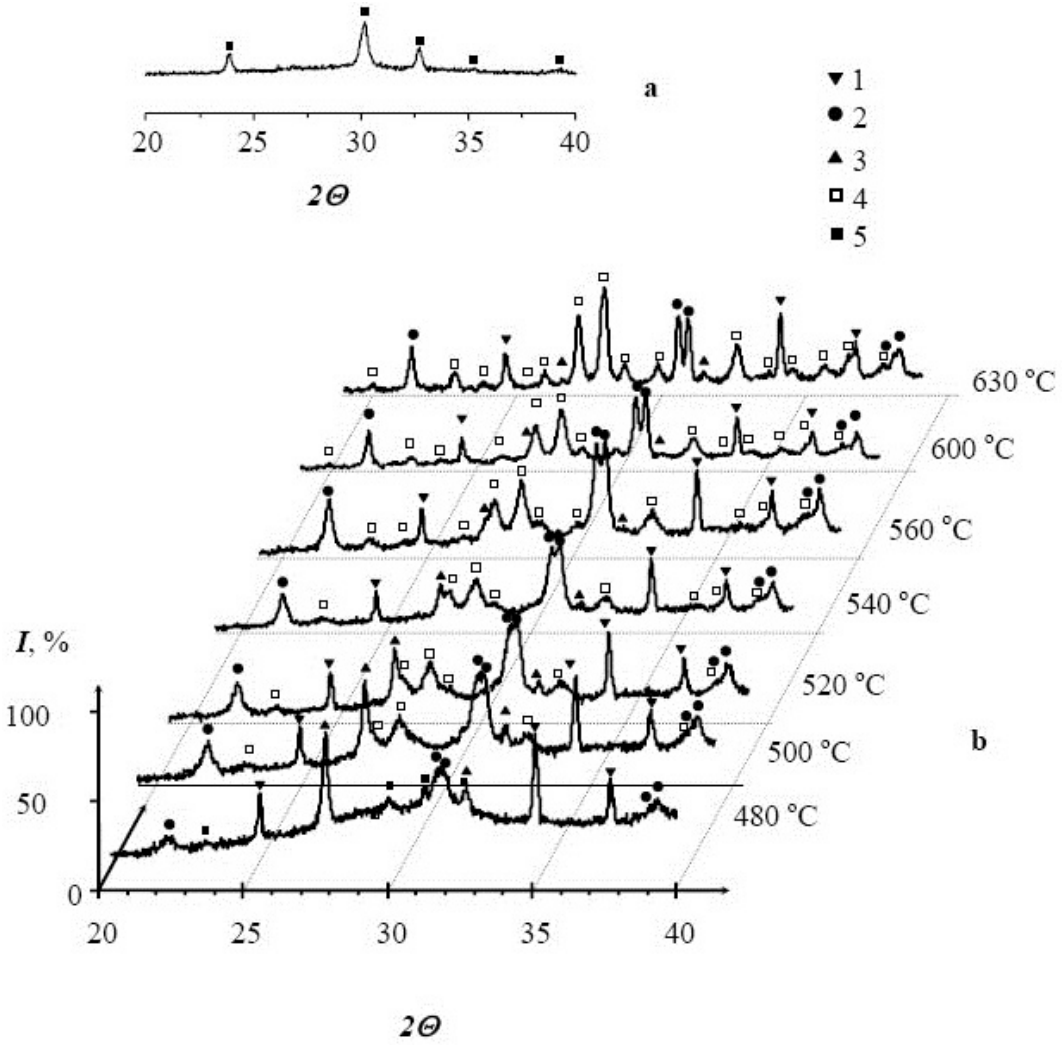


FIG. 1. X-ray diffractograms ($\lambda = 1.54056$ Å): *a* – initial sample; *b* – sample after thermal treatment (1 – $Al_2O_3$, 2 – $BiFeO_3$, 3 – $Bi_{25}FeO_{39}$, 4 – $Bi_2Fe_4O_9$, 5 – $Bi(OH)_3$)

Analysis of the data in Figs. 2, 3 suggests the below-described mechanism of phase formation in the mixture of coprecipitated bismuth and iron hydroxides. Obviously, the pH values of bismuth- and iron hydroxide precipitation under the applied conditions of coprecipitation differed so significantly that the precipitating components were segregated (Fig. 4). This was confirmed by the initially-obtained $Bi(OH)_3$ nanocrystallites (Fig. 1a). Segregation strengthens during thermal treatment due to the difference in dehydration temperatures for the components (Fig. 2).

Bismuth hydroxide dehydration in the presence of an amorphous iron oxide at temperatures around 250 °C was accompanied by the active formation of sillenite-structure bismuth oxide nanoparticles with a chemical formula that can obviously be written in this case as $Bi_{25}FeO_{39}$ (Fig. 3). As the temperature increased, the sillenite-structure bismuth oxide nanocrystals kept growing and reduced in number. This process is most prominent at 480 °C or slightly below (Fig. 3). It should be noted that this temperature range correlates well with the temperature of particles surface transition into a liquid-like state [43, 44], i.e., with the temperature of the

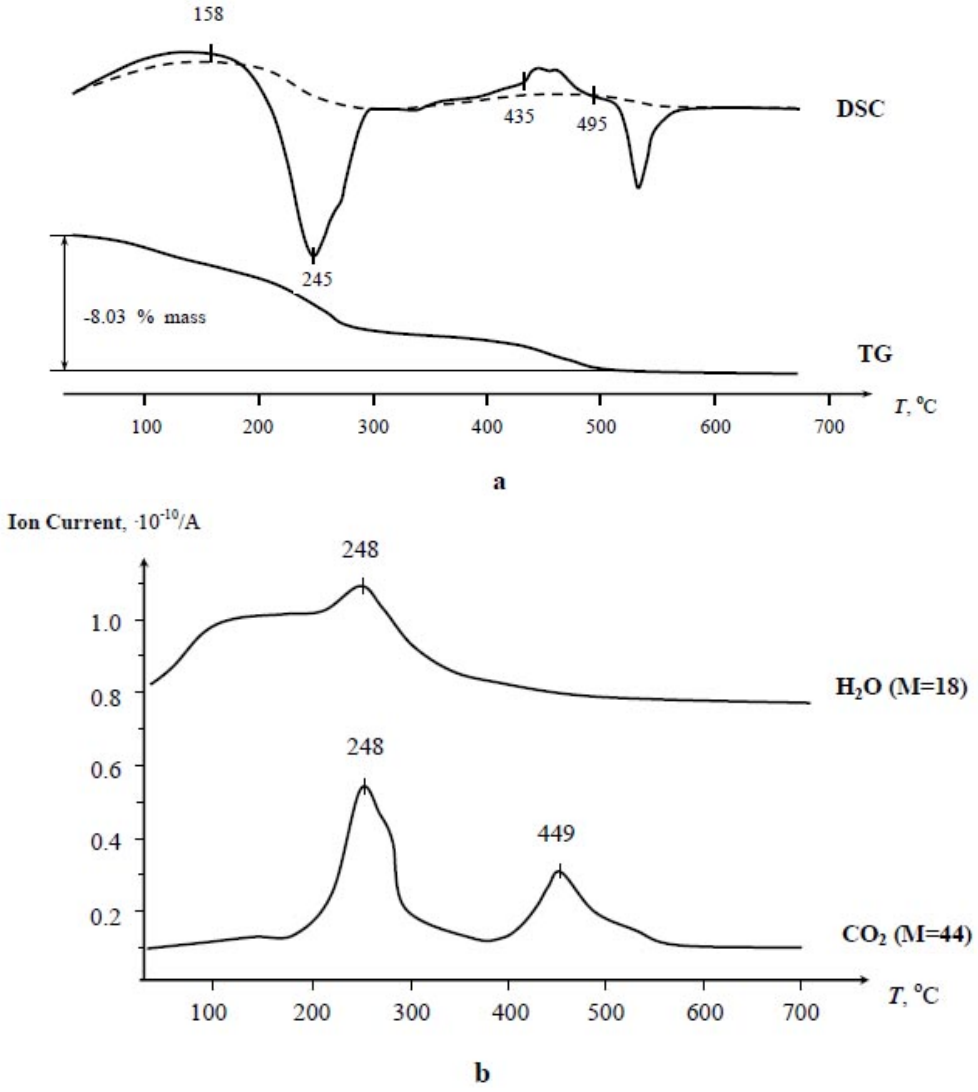


FIG. 2. Temperature-dependent a) mass change (TG), heat flow curve (DSC) and b) ion current mass numbers 18 (M=18) and 44 (M=44) of the sample.

bismuth oxide-based nonautonomous phase melting (460±40 °C) [45], at which mass-transfer along grain boundaries is activated [46, 47].

$BiFeO_3$ nanocrystals with 12±2 nm crystallites start forming in the same temperature range. Nanocrystal formation dominates over their growth until 520 °C. At 520–540 °C, $BiFeO_3$ nanocrystal growth begins (Fig. 3), while their total number reduces (Fig. 3). These temperatures correlate with the calculated temperature of the $BiFeO_3$–based nonautonomous phase melting, which occurs at 520±40 °C [45]. Thus, it can be asserted that $BiFeO_3$ crystallites grow in size and reduce in number in the system at temperatures of the $BiFeO_3$–based nonautonomous phase's melting and represent a consequence of mass transfer intensification along the boundaries of $BiFeO_3$ grains.

It should also be noted that the maximum size of sillenite-structure bismuth oxide crystallites and stabilization of their numbers are observed at temperatures around 520 °C (Fig. 3). At higher temperatures, the sillenite-structure bismuth oxide fraction diminishes in the system, not at the expense of the reducing number of crystallites, but due to the decrease in their size resulting from the bismuth oxide/iron oxide interaction which yields $BiFeO_3$ (Fig. 4).

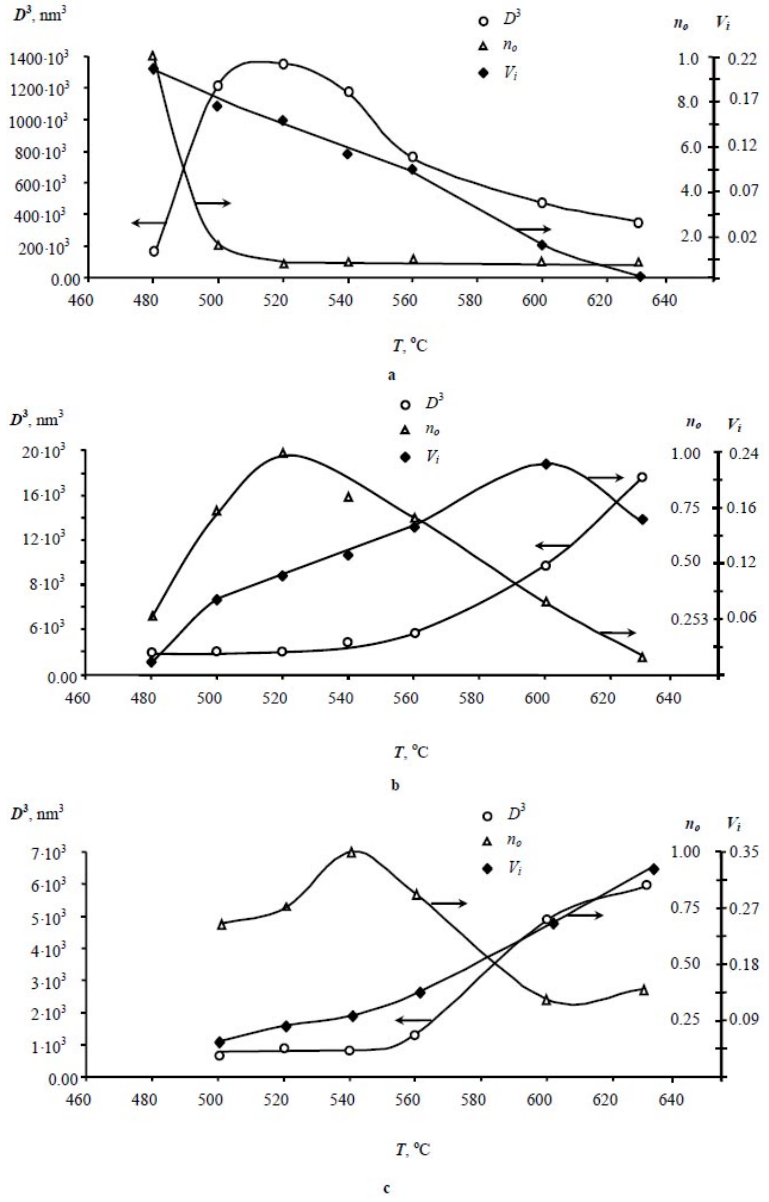


FIG. 3. Changes in crystallites volume ($D^3$) relative to the crystallites number ($n_0$) and volume fraction of the forming phases (a – $Bi_{25}FeO_{39}$, b – $BiFeO_3$, c – $Bi_2Fe_4O_9$) against the increasing temperature of isothermal exposure.

Formation of $Bi_2Fe_4O_9$ nanocrystals was observed only at temperatures around 500 °C and higher (Fig. 3). In this case, crystallites of the formed $Bi_2Fe_4O_9$ were about 6 nm in size, i.e., they were half the size of $BiFeO_3$ crystallites.

The size of crystallites, their number and the fraction of the $Bi_2Fe_4O_9$ phase changed little from 520–560 °C (Fig. 3). A sharp increase in the size of the $Bi_2Fe_4O_9$ crystallites, a decrease in their number and the simultaneous growth of the volume fraction of $Bi_2Fe_4O_9$ in the considered system occurred between 560–600 °C. It should be noted that this temperature range covers the values of the $Bi_2Fe_4O_9$–based nonautonomous phase melting temperature (550±50 °C) calculated on the basis of the expression given in [45]. At temperatures above 600 °C, the $BiFeO_3$ fraction diminished, obviously due to bismuth oxide evaporation and the

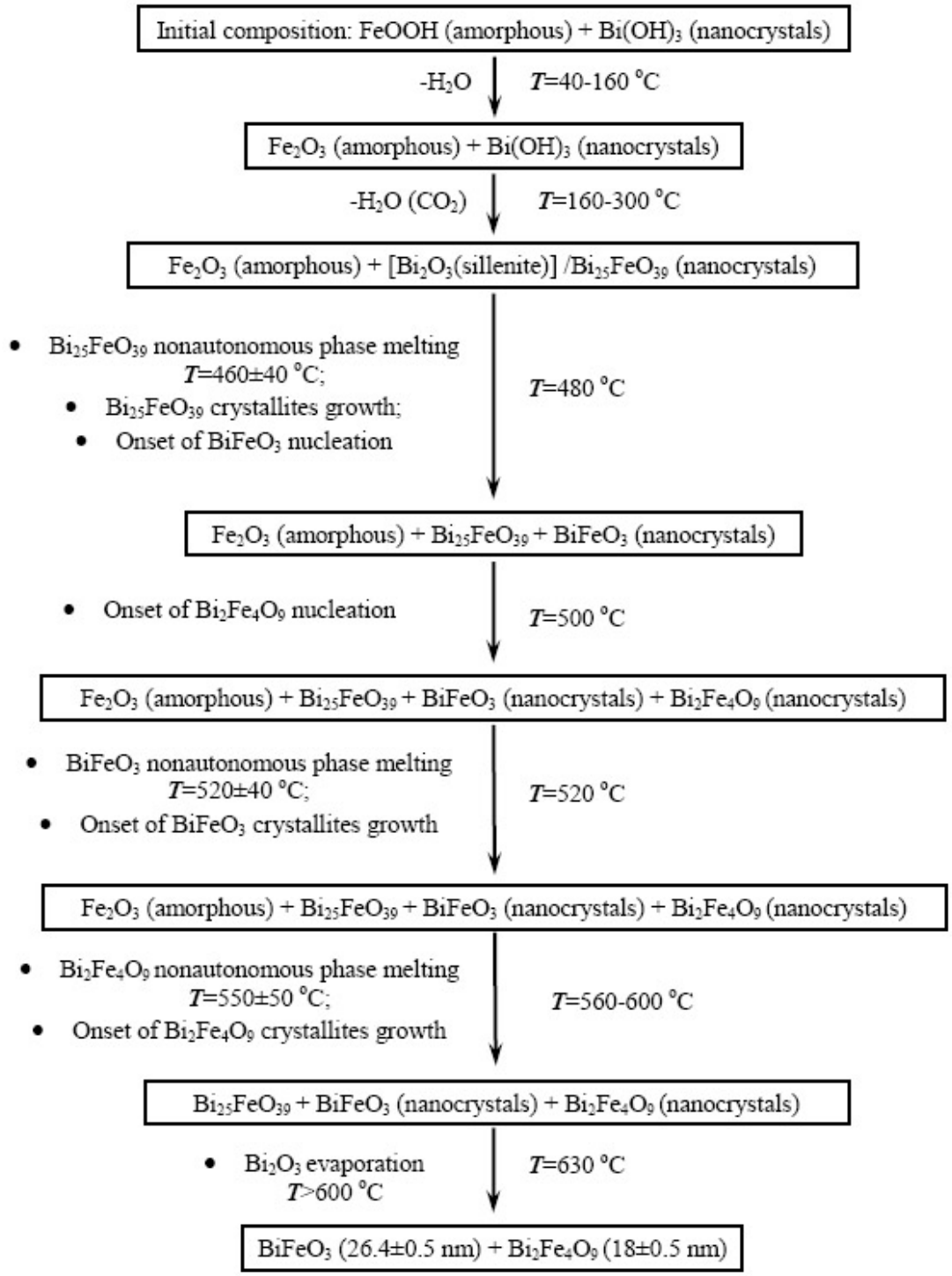


FIG. 4. Transformation in the reaction system. On the left of the arrows – descriptions of processes; on the right – temperature at which transformation was recorded.

respective growth of the $Fe_2O_3$ fraction in the system (Fig. 3), which resulted in the active formation of $Bi_2Fe_4O_9$.

Thus, the mechanism of $BiFeO_3$ formation from a mixture of coprecipitated bismuth and iron hydroxides may be described as a series of elementary transformations presented in Fig. 4. It follows from the analysis of the obtained results that in order to obtain nanocrystalline $BiFeO_3$, the initial composition should be formed with the maximum possible degree of dispersion of reagents evenly spread within the reacting system, and that the temperature of bismuth and iron hydroxides' thermal treatment should be kept within a sufficiently narrow temperature range, 480–520 °C. All these conditions met, it may be expected that the produced nanocrystalline $BiFeO_3$ will contain the least amount of impurity phases.

## 4. Conclusion

Analysis of the sintering temperature for co-precipitated bismuth and iron hydroxides on the formation of $BiFeO_3$ nanoparticles has shown that the transition of nonautonomous phases into a liquid-like state has a decisive influence on the processes of nucleation and crystal growth. The process of $BiFeO_3$ nucleation is activated in the temperature range that corresponds to the transition of the bismuth oxide-based nonautonomous phase into a liquid-like state. The reason is that the area of components contact broadens due to the increased mass transfer rate at the bismuth oxide surface. The growth of $BiFeO_3$ crystals is activated at the temperature of the $BiFeO_3$–based nonautonomous phase melting, which is related to the increased mass transfer rate along grain boundaries at their transition into a liquid-like state.

Therefore, the optimal temperature range for the formation of $BiFeO_3$ nanoparticles from the coprecipitated hydroxides with nanosized particles of the starting materials is from 460–520($\pm$40) °C. The temperature of $BiFeO_3$ nanoparticles synthesis can be reduced only when the initial composition features a much higher degree of spatial contact between components. When raising the temperature of synthesis above the mentioned upper value, it is necessary to decrease the sintering time significantly in order to keep the size of the formed $BiFeO_3$ crystals within the nanosize range.

## Acknowledgment

The reported study was partially supported by RFBR, research project No. 12-08-31453 mol_a.

## References

[1] G.A. Smolenskii, V.A. Isupov, Ferroelectromagnets. *Physics-Uspekhi,* **137**, P. 415–435 (1982).
[2] J. Wang, J. B. Neaton, et al. Epitaxial $BiFeO_3$ Multiferroic Thin Film Heterostructures. *Science,* **299**, P. 1719–1722 (2003).
[3] Y.P. Wang, G.L. Yuan, et al. Electrical and magnetic properties of single-phased and highly resistive ferroelectromagnet $BiFeO_3$ ceramic. *J. Phys. D: Appl. Phys,* **39**, P. 2019–2023 (2006).
[4] T. Choi, S. Lee, et al. Switchable ferroelectric diode and photovoltaic effect in $BiFeO_3$. *Science*, **324**, P. 63–68 (2009).
[5] S.Y. Yang, L.W. Martin, et al. Photovoltaic effects in $BiFeO_3$. *Appl. Phys. Lett*., **95**, P. 062909 (2009).
[6] H.T. Yi, T. Choi, et al. Mechanism of the switchable photovoltaic effect in ferroelectric $BiFeO_3$. *Adv. Mater.,* **23**, P. 3403–3408 (2011).
[7] A.P. Pyatakov, A. K. Zvezdin. Magnetoelectric and multiferroic media. *Physics-Uspekhi*, **55**, P. 557–581 (2012).
[8] S. Li, R. Nechache, C. Harnagea, L. Nikolova, F. Rosei. Single-crystalline $BiFeO_3$ nanowires and their ferroelectric behavior. *Appl. Phys Lett*., **101**, P. 192903–192908 (2012).
[9] H.W. Chang, F.T. Yuan, et al. Photovoltaic property of sputtered $BiFeO_3$ thin films. *J. All. Comp.*, **574**, P. 402–406 (2013).

[10] N.A. Lomanova, V.V. Gusarov. On the limiting thickness of the Perovskite-like block in the Aurivillius phases in the $Bi_2O_3$–$Fe_2O_3$–$TiO_2$ system. *Nanosystems: Physics, Chemistry, Mathematics*, **2**(3), P. 93–101 (2011).
[11] Z. Li, Y. Shen, et al. Significant enhancement in the visible light photocatalytic properties of $BiFeO_3$–graphene nanohybrids. *J. Mater. Chem. A*, **1**, P. 823–829 (2013).
[12] J. Silva, A. Reayes, et al. $BiFeO_3$: A Review on Synthesis, Doping and Crystal Structure. *Integrated Ferroelectrics*, **126**, P. 47–59 (2011).
[13] J. Lu, L.J. Qiao, P.Z. Fu, Y.C. Wu. Phase equilibrium of $Bi_2O_3$–$Fe_2O_3$ pseudo-binary system and growth of $BiFeO_3$ single crystal. *J. Cryst. Grow,* **318**, P. 936–941 (2011).
[14] A. Maitre, M. Francois, J.C. Gachon. Experimental study of the $Bi_2O_3$–$Fe_2O_3$ pseudo-binary system. *J. Phase Equilibria and Diffusion*, **25**, P. 59–67 (2004).
[15] R. Haumont, R. Saint-Martin, C. Byl. Centimeter-size $BiFeO_3$ single crystals grown by flux method. *Phase Transitions*, **81**, P. 881–888 (2008).
[16] R. Palai, R. S. Katiyar, et al. $\beta$ phase and $\beta$-$\gamma$ metal-insulator transition in multiferroic $BiFeO_3$. *Phys. Rev. B*, **77**, P. 014110.1–01410.11 (2008).
[17] E.I. Speranskaya, V.M. Skorikov, E.Ya. Rode, V.A. Terekhova. The phase diagram of the system $Bi_2O_3$–$Fe_2O_3$. *Izv. Bull. Acad. Sci. USSR, Div Chem. Sci.*, **5**, P. 905–906 (1965).
[18] M.I. Morozov, N.A. Lomanova, V.V. Gusarov. Specific Features of $BiFeO_3$ Formation in a mixture of bismuth(III) and iron(III) oxides. *Russ. J. Gen. Chem.,* **73**, P. 1676–1680 (2003).
[19] M. Valant, A.-K. Axelsson, N. Alford. Peculiarities of a Solid-State Synthesis of Multiferroic Polycrystalline $BiFeO_3$. *Chem. Mater*., **19**, P. 5431–5436 (2007).
[20] S.M. Selbach, M.-A. Einarsrud, T. Grande. On the Thermodynamic Stability of $BiFeO_3$. *Chem. Mater*., **21**, P. 169–173 (2009).
[21] S. Phapale, R. Mishra, D. Das. Standard enthalpy of formation and heat capacity of compounds in the pseudo-binary $Bi_2O_3$–$Fe_2O_3$ system. *J. Nuclear Mater*., **373**, P. 137–141 (2008).
[22] A.V. Mikhailov, A. R. Kaul, et al. Mass spectrometric investigation of vaporization in the $Bi_2O_3$–$Fe_2O_3$ system. *Russ. J. Phys. Chem. A*, **85**, P. 26–30 (2011).
[23] M.S. Bernardo, T. Jardiel, et al. Sintering and microstuctural characterization of $W^{6+}$, $Nb^{5+}$ and $Ti^{4+}$ iron-substituted $BiFeO_3$. *J. Eur. Cer. Soc*., **31**, P. 3047–3053 (2011).
[24] A.V. Egorisheva, T.B. Kuvshinova, et al. Synthesis of high nanocrystalline $BiFeO_3$. *Inorgan. Mater.*, **49**, P. 316–320 (2013).
[25] A.V. Egorisheva, T.B. Kuvshinova, et al. Mechanochemical activation of the starting components for the solid phase synthesis of $BiFeO_3$. *Inorgan. Mater.*, **49**, P. 308–315 (2013).
[26] S. Das, S. Basu. Solvothermal synthesis of nano-to-submicrometer sized $BiFeO_3$ and Bi-Fe-oxides with various morphologies. *J. Nanosci. Nanotechnol*., **9**, P. 5622–562 (2009).
[27] J.-H. Xu, H. Ke, et al. Low-temperature synthesis of $BiFeO_3$ nanopowders via a sol–gel method. *J. All. Comp*., **472**, P. 473–477 (2009).
[28] B. Liu, B. Hu, Z. Du. Hydrothermal synthesis and magnetic properties of single-crystalline $BiFeO_3$ nanowires. *China Chem. Comm*., **47**, P. 8166–8168 (2011).
[29] J. Yang, X. Li, et al. Factors controlling pure-phase magnetic $BiFeO_3$ powders synthesized by solution combustion synthesis. *J. All. Comp*., **509**, P. 9271–9277 (2011).
[30] D. Maurya, H. Thota, K. S. Nalwa, A. Garg. $BiFeO_3$ ceramics synthesized by mechanical activation assisted versus conventional solid-state-reaction process: A comparative study. *J. All. Comp*., **477**, P. 780–784 (2009).
[31] M.M. Rashad. Effect of synthesis conditions on the preparation of $BiFeO_3$ nanopowders using two different methods. *J. Mat. Sci.: Materials in Electronics*, **23**, P. 882–888 (2012).
[32] A. Chaudhuri, S. Mitra, M. Mandal, K. Mandal. Nanostructured bismuth ferrites synthesized by solvothermal process. *J. All. Comp*., **491**, P. 703–706 (2010).
[33] M. Popa, D. Crespo, J.M. Calderon-Moreno, S.F. Preda. Synthesis and Structural Characterization of Single-Phase $BiFeO_3$ Powders from a Polymeric Precursor. *J. Am. Cer. Soc*., **90**, P. 2723–2727 (2007).
[34] A. Hardy, S. Gielis, et al. Effects of precursor chemistry and thermal treatment conditions on obtaining phase pure bismuth ferrite from aqueous gel precursors. *J. Eur. Cer. Soc.*, **29**, P. 3007–3013 (2009).
[35] Sh. Shetty, V. R. Palkar, R. Pinto. Size effect study in magnetoelectric $BiFeO_3$ system. *J. Phys*., **58**, P. 1027–1030 (2002).
[36] J.-H. Xu, H. Ke, et al. Factors controlling pure-phase multiferroic $BiFeO_3$ powders synthesized by chemical co-precipitation. *J. All. Comp*., **472**, P. 473–477 (2009).
[37] J. Prado-Gonjal, M.E. Villafuerte-Castrejorn, L. Fuentes, E. Morarn. Microwave–hydrothermal synthesis of the multiferroic $BiFeO_3$. *Mat. Res. Bull.*, **44**, P. 1734–1737 (2009).

[38] V. Kothai, R. Rajeev. Synthesis of $BiFeO_3$ by carbonate precipitation. *Bull. Mat. Sci*., **35**, P. 157–161 (2012).
[39] B. Jurca, C. Paraschiv, A. Ianculescu, O. Carp. Thermal behaviour of the system $Fe(NO_3)_3{\cdot}9H_2O$–$Bi_5O(OH)_9(NO_3)_4{\cdot}9H_2O$–glycine/urea and of their generated oxides ($BiFeO_3$). *J Therm. Anal. Calor*., **97**, P. 91–98 (2009).
[40] Quantitative analysis code. Registration certificate No. 2000611264 of 06.12.2000. PDWin-4.0. bundled software, "Burevestnik" Scientific and Production Association. St. Petersburg. 2004 24.
[41] T. Misawa, K. Hashimoto, S. Shimodaira. The mechanism of formation of iron oxide and oxy-hydroxides in aqueous solutions at room temperature. *Corros. Sci*., **14**, P. 131–135 (1974).
[42] V.M. Denisov, N.V. Belousova, et al. Oxide compounds of $Bi_2O_3$–$Fe_2O_3$ system I. The obtaining and phase equilibriums. *J. Siberian Federal University. Chemistry*, **5**, P. 146–167 (2012).
[43] J.G. Dash. Surface melting. *Contemp. Phys*., **30**, P. 89–100 (1989).
[44] V.V. Gusarov, S.A. Suvorov. Melting-points of locally equilibrium surface phases in polycrystalline systems based on a single volume phase. *Journal of Applied Chemistry of the USSR*, **63**(8), P. 1560–1565 (1990).
[45] V.V. Gusarov. The thermal effect of melting in polycrystalline systems. *Thermochimica Acta*. **256**, P. 467–472 (1995).
[46] V.V. Gusarov, I.Yu. Popov. Flows in two-dimensional non-autonomous phases in polycrystalline systems. *Nuovo Cimento della Societa Italiana di Fisica. D*, **18**(7), P. 799–805 (1996).
[47] V.V. Gusarov. Fast solid-phase chemical reactions. *Russian Journal of General Chemistry*, **67**(12), P. 1846–1851 (1997).